Theoretical Beam Hardening Correction for Industrial X-ray Computed Tomography

Osama M.H. Ahmed[1,2], YuShou Song[1,*] & Zhaoyang Xie[1]

[1]College of Nuclear Science and Technology, Harbin Engineering University, 145 Nantong Street, Nangang District, Harbin China, 150001
[2]Chemistry and Nuclear Physics Institute, Sudan Atomic Energy Commission, Gamma Street, P.O. Box 3001 Khartoum, Sudan
*E-mail: songyushou80@163.com

Abstract. Beam hardening is a significant artifact that comes from the polychromatic nature of the X-ray source in computed tomography. It appears because the object tends to absorb more low-energy photons within the beam, which leads to a nonlinear relationship between attenuation and material thickness. As a result, the reconstructed image is spoiled. This work articulates an approach to promoting the correction of beam hardening at MeV X-ray. In order to calculate the attenuation of the polychromatic beam, the following terms were evaluated: the energy spectra S(E) for sets of X-ray spectra with a maximum energy of 2, 4, 6 and 9 MeV were simulated using the Geant4 toolkit; the counting efficiency λ(E) was estimated based on the Lifton method; and the attenuation coefficient μ(E) was taken from the NIST database. The non-linear relationship between the attenuation and the thickness of iron was investigated. The beam hardening for each energy set was successfully corrected by polynomial fitting, that transforming the polychromatic attenuation data into equivalent monochromatic data. The corrected attenuation was used to estimate the penetration capability of the X-ray source and produced a result that was consistent with what has been reported in the literature.

Keywords: *beam hardening; computed tomography; X-ray attenuation; counting efficiency; polychromatic X-ray; monochromatic X-ray; polynomial fitting.*

1 Introduction

X-ray computed tomography (XCT) generates 3D images taken of an object at multi-angular positions to present cross-sectional images from a series of 2D images of specific areas that are scanned [1]. XCTs are widely applied in medical diagnostics and since the last decade CT images have been widely adopted in the finite element (FE) modeling of bones. Starting from CT images it is possible to reconstruct a patient-specific geometry of the bone and then derive an FE model to investigate its mechanical behavior through computational simulations in order to predict the fracture risk, especially in the case of pathological bones with compromised strength [2-5]. CT is a vital inspection tool for quality assurance in non-destructive testing, covering a wide

Received June 12th, 2019 1st Revision September 2nd, 2019, 2nd Revision November 11th, 2019, Accepted for publication December 2nd, 2019.
 ISSN: 2337-5779, DOI: 10.5614/j.eng.technol.sci.2019.51.6.9

range of industrial applications, such as automobile engines, pressure vessels, building structures, piping, hoisting equipment and so on [6-8], where high-quality images are required.

The essential aim of XCT is to transfer exact points in an object to a final image, where each point is assigned in the final image based on the X-ray attenuation of the object's material [9]. This transfer of information is never perfect due to image artifacts from the image reconstruction processes that affect the image's quality. These artifacts lead to inequality in the CT images, but they can be corrected or eliminated [10,11].

The X-ray source in XCT consists of an extensive range of photon energies, so-called polychromatic X-rays. However, the object tends to absorb more low-energy photons within the beam, thus enabling the beam to become gradually harder, leading to so-called beam hardening artifacts. This results in inaccurate detection of the attenuation coefficient. As a result, the linearity between the attenuation and the material thickness fails where the internal area of an object is traversed by X-rays with energy higher than the edge area, which can make the edges appear more attenuated than the interior regions. This is why objects in tomographic images have shining edges and darker center areas. Where the imaging system cannot accurately record or transfer each point in the object to the final image, causing a significant decrease in imaging quality.

Reconstruction of the image requires an accurate attenuation map of the object under investigation [12]. A variety of methods such as physical filtration [13], dual-energy imaging [14] alternative reconstruction [15], and polynomial fitting [9] have been used for correcting attenuation errors or beam hardening. Polynomial fitting is a software-based method developed by Herman [9] that transforms the attenuation data of a polychromatic beam, which is a curved function, into equivalent attenuation data of a monochromatic beam, i.e. a linear function. Then, polynomial regression is applied to get the corrected attenuation data. The polynomial fitting method (linearization) is a more comprehensive and widely used for industrial CT. It requires full knowledge about the characterization of the material and the energy spectrum, which in brief includes all of the models discussed in Ahmed and Song [16]. A recent work concentrating on corrected beam hardening for a multi-material object without considering prior knowledge about the X-ray spectrum and material composition [16].

In this work, theoretical correction of MeV X-ray attenuation or beam hardening is described. The Geant4 based Monte Carlo (MC) code was used to simulate a linear accelerator X-ray source, producing Bremsstrahlung X-rays at different accelerated electron energies. The polychromatic attenuation data and

the equivalent monochromatic attenuation data for iron (Fe) were numerically calculated, after which the errors in the attenuation (beam hardening) were corrected.

2 Material and Methods

This work articulates an approach to promoting the correction of beam hardening of X-rays at MeV. The simulation and theoretical calculations were performed in three steps: first, the Geant4 Monte Carlo (MC) code was used for simulating the linear electron accelerator driving an X-ray source that produces Bremsstrahlung at MeV energy. Secondly, the attenuation data of the polychromatic X-ray and equivalent monochromatic attenuation data were numerically calculated according to the Beer-Lambert law. Then, beam hardening correction was carried out using the polynomial fitting method. Finally, the obtained results were validated with the literature.

2.1 X-ray Source Simulation

Geant4 is an object-oriented C++ version toolkit for Monte Carlo simulation that was developed at CERN by high-energy physics professionals to simulate the passage of particles through matter [17, 18]. It consists of physics models for describing the electromagnetic and hadronic interactions of many kinds of particles, including neutron, positrons, and photons. It can be applied in different areas of physics, including high-energy physics, astrophysics, nuclear and accelerator physics, medical physics, and radiation physics [19].

The Geant4 Monte Carlo code, version GEANT4.10.03.p02, was used for simulating Bremsstrahlung emission from a linear electron accelerator driving the X-ray source, where X-ray beams are produced by electron kinetic energy that decelerate in metallic targets. A fraction of the electron kinetic energy in the target is transformed into heat and a fraction of the energy is emitted in the form of Bremsstrahlung photons. For this purpose, 1×10^6 monochromatic electrons parallel to the Z-direction with energies of 2, 4, 6 and 9 MeV hit a tungsten (W) target of which the thickness was assumed to be the maximum range of an electron in tungsten, as obtained from the NIST database (see Table l).

Table 1 Maximum electron range in tungsten.

Accelerated energy (MeV)	Maximum range (g/cm^2)
2	2.002
4	3.059
6	4.265
9	5.770

In the simulation, Bremsstrahlung photons and secondary particles were produced, the outgoing beam was collimated in such way that it adopted a fan beam shape and a surface detector was placed at a distance from the target to count the photons. The energy spectra of the photon beams were obtained as one of the essential terms for attenuation calculations. Figure 1 shows the energy spectra at 2, 4, 6 and 9 MeV as function of photon count.

2.2 X-ray Attenuation Calculation

The attenuation of X-ray beams that are passed through an object can be calculated by assuming that the object has been placed in a fixed position between the X-ray source and the detector. The attenuation coefficients at any point inside the volume of an object depend on the location (x, y) and the X-ray energy.

A monochromatic beam has fixed energy $\bar{E}$ and the number of photons generated by the source is (N_0), which can pass the object's material with linear attenuation coefficient μ(E) and path length of (L) to the detector. Therefore, the monochromatic attenuation (M_L) can be calculated according to the Beer-Lambert law of attenuation, as given below:

$$M_L = -\ln \frac{N}{N_0} = \mu_{eff}(x,y,\bar{E})l \quad (1)$$

where μ_{eff} is the effective attenuation coefficient, which is used to denote the energy independent attenuation coefficient, i.e. the effective energy of the polychromatic system. It can be numerically computed by Eq. (2) [20] when prior information about the material composition and energy spectrum S(E) is known, which can be written as:

$$\mu_{eff}(\overline{E}) = \frac{\int \mu(E)S(E)dE}{\int S(E)dE} \quad (2)$$

The X-ray beam in all computed tomographies is polychromatic for a specific source-detector pair position and therefore polychromatic attenuation P_L can be calculated using the following equation:

$$P_L = -ln\frac{N}{N_0} = -ln\frac{\int S(E)\lambda(E)exp-\int \mu(x,y,E)dLdE}{\int S(E)\lambda(E)dE} \quad (3)$$

where S(E) is the initial X-ray energy spectrum and λ(E) is the counting efficiency.

For the evaluation of Eqs. (1) and (3) full information about each term is required: the energy spectrum S(E) was already obtained from the X-ray source simulation, the μ(E) coefficient values were obtained from the NIST database

[21], and counting efficiency λ(E) was evaluated using the Lifton method, [22] which will be discussed in the following section.

2.2.1 Efficiency Estimation

In order to estimate the counting efficiency function, λ(E), the Lifton method in [22] was used, where Eq. (3) is rearranged by considering $\int S(E)\lambda(E) = 1$ (in the denominator). Thus, the X-ray transmission N/N_0 can be written as a series of linear equations in the form of Ax = b. Assuming that

$$A = \exp[-\mu(E)l],\ x = T(E),\ ,\ b = N/N_0,$$

then

$$N/N_0 = T(E)exp[-\mu(E)l], \tag{4}$$

where

$$\lambda(E) = T(E)/S(E) \tag{5}$$

Matrix A has a dimension of $(n \times m)$. Each entity of this matrix is written as exp[-μ(E)l. Matrix X ($with\ a\ dimension\ of\ 1 \times m$) contains the entity factors $T(E_i)$ that are defined as source-detector efficiency. $T(E_i)$ equals energy spectrum $S(E)$ multiplied by counting efficiency λ(E) for a specific energy bin. Column matrix b of size $(1 \times m)$ contains the transmission of X-ray attenuators (N/N_0), which can be obtained by Eq. (4). Therefore, the final form of the rearrangement of Eq. (4) can be written as:

$$\begin{bmatrix} \exp(-\mu_1 l_1) & \exp(-\mu_2 l_1) & \dots & \exp(-\mu_m l_1) \\ \vdots & \vdots & & \vdots \\ \exp(-\mu_1 l_n) & \exp(-\mu_2 l_n) & \dots & \exp(-\mu_n l_m) \end{bmatrix} \begin{bmatrix} T(E_1) \\ \vdots \\ T(E_m) \end{bmatrix} = \begin{bmatrix} N_1/N_0 \\ \vdots \\ N_n/N_0 \end{bmatrix} \tag{6}$$

To obtain a solution for the above system, let us suppose that we have seventeen different iron foils, each of which has a thickness of 3 cm. They are stacked and irradiated by X-rays with a maximum energy spectrum of 9 MeV. The whole thickness may vary from 3 to 51 cm. The X-ray transmission is calculated for each subsequent exposure, 3 cm of iron is added. The value of μ(E) is taken from the NIST XCOM database. The initial energy spectrum S(E) is obtained from the X-ray source simulation in Figure 1(d).

The solution was obtained by using the least squares approximation for the system equations, which can give the best approximation of T(E). After estimating the values of T(E) in Eq. (6), the function λ(E) can be evaluated by Eq. (5) and consequently the polychromatic attenuation can be calculated using Eq. (3). Figure 2 shows the counting efficiency as a function of incident photon energy, which was obtained using Eq. (5).

2.3 Beam Hardening Correction

For the beam hardening correction using linearization or polynomial fitting, firstly, the attenuation of a polychromatic X-ray in iron for a maximum energy spectrum of 2, 4, 6, and 9 MeV, respectively, was numerically calculated using Eq. (3). Its terms were obtained in the sections above. The same data for iron thickness and attenuation coefficient were used as in the energy efficiency estimation. Secondly, the equivalent monochromatic attenuation data were calculated using Eq. (1). The correction was achieved by normalizing the polychromatic attenuation data with the equivalent monochromatic attenuation data and then applying polynomial fitting regression to get the corrected attenuation values.

3 Results

Figure 1 shows the energy spectrum of the 1×10^6 electron.mm^{-2} that hit the tungsten target with 2, 4, 6, and 9 MeV acceleration energy from a-d respectively.

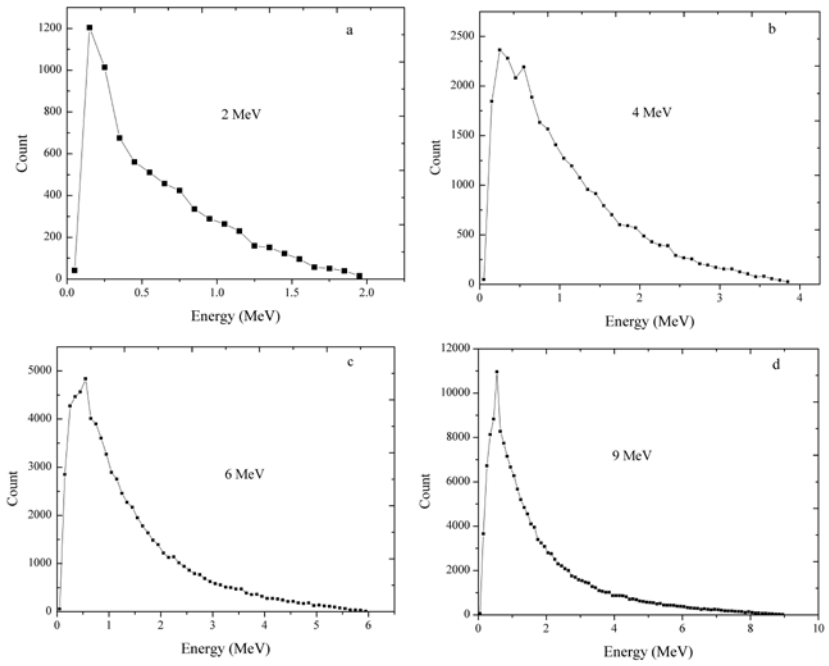

Figure 1 The energy spectrum of the $1x10^6$ electron.mm^{-2} that hit the tungsten target with 2, 4, 6, and 9 MeV acceleration energy from a-d respectively.

Figure 2 shows the counting efficiency as a function of incident photon energy and Figure 3 shows the calculated attenuation curves for iron (Fe) at 2, 4, 6, and 9 MeV energy spectra vs. iron thickness. The relative error in the attenuation was also evaluated and corrected by 8-degree polynomial fitting. Table 2 shows the attenuation of the selected thickness for iron before and after beam hardening correction of the discrete energy spectrum. Finally, Figure 3 shows the change of the transmission X-ray versus iron thickness for all the selected energies.

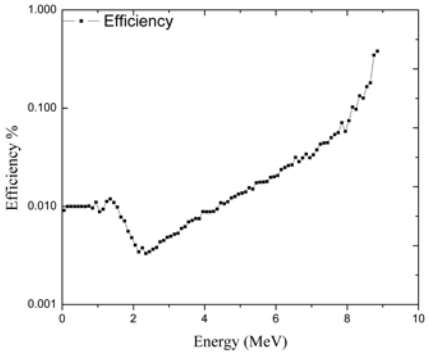

Figure 2 Counting efficiency as a function of incident photon energy.

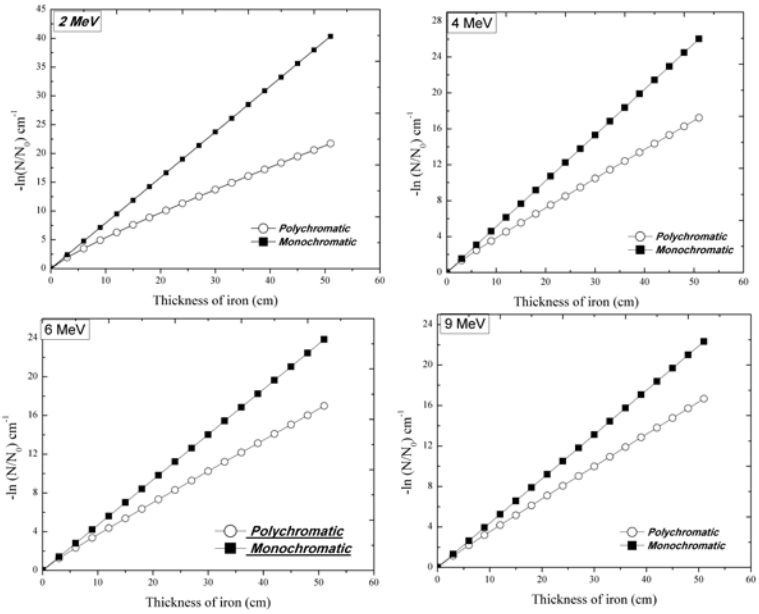

Figure 3 Calculated attenuation curves for iron (Fe) at 2, 4, 6, and 9 MeV energy spectra vs. iron thickness.

Table 2 Attenuation of selected thickness for iron before and after correction of the discrete energy spectrum.

Energy (MeV)	Thickness (cm)	μ (cm^{-1})		Relative error %
		Before correction	After correction	
2	3	1.9215244	1.915814224	-0.298
	9	4.9067839	4.907494589	0.014
	15	7.5846977	7.590048843	0.071
4	3	1.334216516	1.331073943	-0.236
	15	5.53858158	5.540535948	0.035
	24	8.508229985	8.535292416	0.317
6	3	1.246403331	1.244118705	-0.184
	18	6.351631548	6.36758813	0.251
	27	9.27779858	9.371694103	1.002
9	3	1.147906733	1.138637481	-0.814
	21	7.098412786	7.097831929	-0.008
	33	10.94060395	10.96010463	0.178

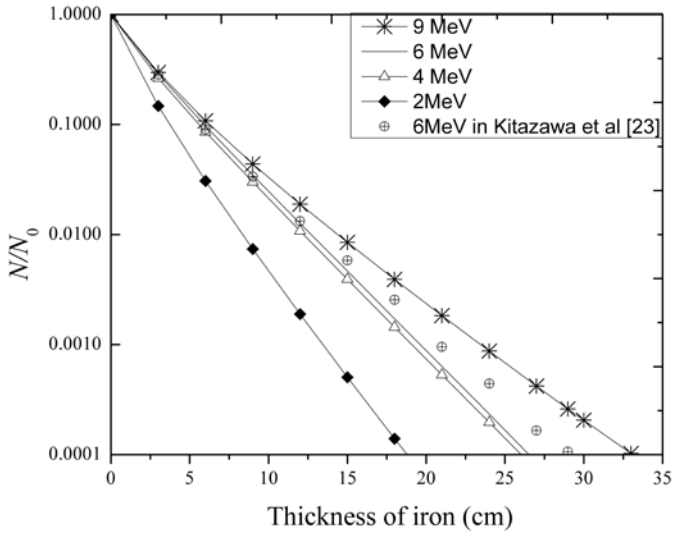

Figure 4 Corrected X-ray transmission versus iron thickness.

4 Discussion

In order to calculate the attenuation in Eqs. (1) and (3), three essential terms were obtained: linear attenuation coefficient μ(E), energy spectrum S(E), and

counting efficiency λ(E). The value of μ (E) was obtained from the NIST database [21] and the energy spectrum S(E) was simulated. Figure 1 shows the change of photon count for the 2, 4, 6, and 9 MeV energy spectra. The obtained spectra indicate a positive correlation between the count and the accelerated electron energies. The counting efficiency λ(E) was evaluated using the Lifton method, as described in Section 2.2.1. Figure 2 shows the counting efficiency as a function of incident photon energy. The monochromatic attenuation and the polychromatic attenuation were calculated using Eqs. (1) and (3). Figure 3 shows the calculated X-ray attenuation curves of iron (Fe) at 2, 4, 6, and 9 MeV energy spectra, both monochromatic and polychromatic. It can clearly be seen that the polychromatic attenuation has a non-linear relationship with material thickness due to the beam hardening effect. The procedure for correcting the beam hardening effect was adopted from Herman [9]. The polychromatic attenuation data (P_L) and the monochromatic attenuation data (M_L) are shown in Figure 3. The relation between M_L and PL was obtained by plotting M_L versus P_L and applying 8-degree polynomial fitting for normalization, as shown in Eq. (7):

$$M_L=a_n P_L{}^n+a_{n-1}P_L^{n-1}+\ldots+a_0+\text{intercept} \tag{7}$$

This fitting function was applied to the original attenuation data to normalize them with the equivalent monochromatic attenuation data of the object under study. Table 2 shows the attenuations of selected thicknesses of iron before and after correction of the discrete energy spectra. The relative error in the attenuation was evaluated using Eq. (8).

$$\text{R. E \%}= \frac{\text{attenuation after correction-attenuation before correction}}{\text{attenuation after correction}} \text{ x } 100\% \tag{8}$$

The corrected X-ray transmission was plotted versus iron thickness; the penetration thickness for 2, 4, 6 and 9 MeV X-ray energy spectra were investigated; Figure 4 shows the corrected X-ray transmission at 2, 4, 6, and 9 MeV energy spectra versus iron thickness; the maximum thickness was found to be about 18 cm, 27 cm, 28 cm, more than 30 cm at 2, 4, 6, and 9 MeV respectively. The probative value of penetration thickness at 6 MeV was obtained from Kitazawa, *et al.* [23] and compared with our work for validation. The penetration thickness could be used for the estimation of the object size for actual X-ray source capability.

5 Conclusion

This work presents an approach to promoting the correction of X-ray attenuation due to beam hardening in CT applications. A linear electron accelerator driving the X-ray source was modeled using Geant4. The

Bremsstrahlung produced by this accelerator had X-ray spectra with a maximum energy of 2, 4, 6, and 9 MeV. For the X-rays with the different spectra, the attenuations of polychromatic X-rays in iron were numerically calculated. The non-linear relationship between attenuation and iron thickness was investigated. Beam hardening was successfully corrected using polynomial fitting, where the polychromatic attenuation data were transformed into equivalent monochromatic attenuation data. The attenuation correction of iron for the energy spectra mentioned above was used to obtain the penetration thickness, which can serve for selecting the object size according to the source penetration capability.

In the future, further research can be conducted to find a new approach to correct beam hardening for multi-material objects without the need to perform segmentation and without considering prior knowledge about the X-ray spectrum and material composition. In the medical field, finite element modeling of CT images is used for density estimation, which requires the measurement of the object (segmentation). A finite element model can also be considered as a future direction for correcting beam hardening in industrial applications.

Acknowledgments

This work was supported by the Fundamental Research Funds for the Central Universities of China. The authors would also like to express their thanks to Mr. Silmam and Mr. Taher for their help.

References

[1] Arunmuthu, K., Ashish, M., Saravanan, T., Philip, J., Rao, B.P.C. & Jayakumar, T., *Simulation of Beam Hardening in X-Ray Tomography and Its Correction Using Linearisation and Pre-filtering Approaches, Insight Non-Destructive Test*, Cond. Monit., **55**(10), pp. 540-547, 2013.

[2] Shimizu, Y., Usui, K., Araki, K., Kurosaki, N., Takanobu, H. & Takanishi, A., S*tudy of Finite Element Modeling from CT Images*, Dent. Mater. J., **24**(3), pp. 447-455, 2005.

[3] Amir Sternheim, Z.Y., Giladi, O., Gortzak, Y., Drexler, M., Salai, M., Trabelsi, N. & Milgrom, C., *Pathological Fracture Risk Assessment in Patients with Femoral Metastases Using CT-based Finite Element Methods, A Retrospective Clinical Study*, Br. J. Psychiatry, **111**(479), pp. 1009-1010, 1965.

[4] Sternheim, A., *Pathological Fracture Risk Assessment in Patients with Femoral Metastases Using CT-Based Finite Element Methods, A Retrospective Clinical Study*, Bone, **110**, pp. 215-220, 2018.

[5] Falcinelli, C., Di Martino, A., Gizzi, A., Vairo, G. & Denaro, V., *Mechanical Behavior of Metastatic Femurs through Patient-Specific Computational Models Accounting for Bone-Metastasis Interaction*, J. Mech. Behav. Biomed. Mater., **93**, pp. 9-22, 2019.

[6] Flisch, A., *Industrial Computed Tomography in Reverse Engineering Applications*, Comput. Tomogr. Image Process, April, pp. 45-53, 1999.

[7] Shammaa, M.H., Ohtake, Y. & Suzuki, H., *Segmentation of Multi-Material CT Data of Mechanical Parts for Extracting Boundary Surfaces*, Comput. Des., **42**(2), pp. 118-128, 2010.

[8] Smith, C.R., Holt, K., Bischoff, U., Georgi, B., Hansen, F. & Jeltsch, F., *Application of 450 Kv Computed Tomography to Engine Blocks with Steel Liners*, Mater. Eval., **65**(5), pp. 458-461, 2007.

[9] Herman, G.T., *Correction for Beam Hardening in Computed Tomography*, Phys. Med. Biol., **24**(1), pp. 81-106, 1979.

[10] Lifton, J.J., *Multi-Material Linearization Beam Hardening Correction for Computed Tomography*, J. Xray. Sci. Technol., **25**(4), pp. 629–640, 2017.

[11] Hanna, R.D. & Ketcham, R.A., *X-Ray Computed Tomography of Planetary Materials: A Primer and Review of Recent Studies*, Chemie der Erde – Geochemistry, **77**(4), pp. 547-572, 2017.

[12] Ramakrishna, K., Muralidhar, K. & Munshi, P., *Beam-Hardening in Simulated X-Ray Tomography*, NDT E Int., **39**(6), pp. 449-457, 2006.

[13] Jennings, R.J., *A Method for Comparing Beam-Hardening Filter Materials for Diagnostic Radiology*, Med. Phys, **15**(4), pp. 588-599, 1988.

[14] Rapaport, M.S., Gayer, A., Iszak, E., Goresnic, C., Baran, A. & Polak, E., *A Dual-Mode Industrial CT*, Nucl. Inst. Methods Phys. Res. A, **352**(3), pp. 652-658, 1995.

[15] Brabant, L., Pauwels, E., Dierick, M., Van Loo, D., Boone, M. A. & Van Hoorebeke, L., *A Novel Beam Hardening Correction Method Requiring No Prior Knowledge*, Incorporated in an Iterative Reconstruction Algorithm, NDT E Int., **51**, pp. 68-73, 2012.

[16] Ahmed, O.M.H. & Song, Y., *A Review of Common Beam Hardening Correction Methods for Industrial X-ray Computed Tomography*, Sains Malaysiana, **47**(8), pp. 1883-1890, Aug 2018.

[17] Guatelli, S., Cutajar, D. & Rosenfeld, A.B., *Introduction to the Geant4 Simulation Toolki*t, May, 2011.

[18] Elvira, V.D., Lebrun, P. & Spentzouris, P., *Beam Simulation Tools for GEANT4 (and Neutrino Source Applications)*, Batavia – USA, 2002.

[19] Agostinelli, S., GEANT4 - *A Simulation Toolkit, Nucl. Instruments Methods Phys. Res. Sect. A Accel. Spectrometers*, Detect. Assoc. Equip., **506**(3), pp. 250-303, 2003.

[20] Gao, H., Zhang, L., Chen, Z., Xing, Y. & Li, S., *Beam Hardening Correction for Middle-Energy Industrial Computerized Tomography*, IEEE Trans. Nucl. Sci., **53**(5), pp. 2796-2807, 2006.
[21] J.H.H. & Seltzer, S.M., *NIST Standard Reference Database 126: X-Ray Mass Attenuation Coefficients*, 2004, https://www.nist.gov/pml/x-ray-mass-attenuation-co.
[22] Lifton, J.J., Malcolm, A.A. & McBride, J.W., *The Application of Beam Hardening Correction for Industrial X-ray Computed Tomography*, in 5th International Symposium on NDT in Aerospace, 2013.
[23] Kitazawa, S., Abe, Y. & Satoh, K., *Simulations of Mev Energy Computed Tomography*, NDT E Int., **38**(4), pp. 275-282, 2005.